Magnetic Resonance in Medicine 45:1021–1029 (2001)

Perfusion Imaging Using Dynamic Arterial Spin Labeling (DASL)

Emmanuel L. Barbier,[1] Afonso C. Silva,[1] Seong-Gi Kim,[2] and Alan P. Koretsky[1*]

Recently, a technique based on arterial spin labeling, called dynamic arterial spin labeling (DASL (Magn Reson Med 1999;41:299–308)), has been introduced to measure simultaneously the transit time of the labeled blood from the labeling plane to the exchange site, the longitudinal relaxation time of the tissue, and the perfusion of the tissue. This technique relies on the measurement of the tissue magnetization response to a time varying labeling function. The analysis of the characteristics of the tissue magnetization response (transit time, filling time constant, and perfusion) allows for quantification of the tissue perfusion and for transit time map computations. In the present work, the DASL scheme is used in conjuction with echo planar imaging at 4.7 T to produce brain maps of perfusion and transit time in the anesthetized rat, under graded hypercapnia. The data obtained show the variation of perfusion and transit time as a function of arterial pCO_2. Based on the data, CO_2 reactivity maps are computed. Magn Reson Med 45:1021–1029, 2001. Published 2001 Wiley-Liss, Inc.†

Key words: cerebral blood flow; cerebral blood volume; MR; frequency filtering; transit time

Dynamic arterial spin labeling (DASL) (1) is a recently introduced MR technique for measuring perfusion based on arterial spin labeling (2–6). DASL allows the simultaneous measurement of three parameters that contribute to the quantification of perfusion: the transit duration of labeled spins from the labeling plane to the tissue, the longitudinal tissue relaxation time, and the amplitude of the signal change induced by the arrival of labeled spins into the voxel. In order to measure these parameters, the DASL scheme measures tissue magnetization response to a periodic labeling function (LF). Using DASL, perfusion is quantified more accurately, since spatial variations in the value of transit time and in the value of tissue longitudinal relaxation time are taken into account (7,8). DASL can also create transit time maps. An accurate determination of the arterial transit time and of the tissue perfusion is important for assessing tissue viability in pathological conditions such as stroke, where blood flow is reduced and blood transit time increased (9), or to characterize the functional response of the cortex during task activation (10).

In the previous work (1), we demonstrated the principles of the DASL method using a volume-localized stimulated-echo acquisition mode sequence (11), and we verified that the values of perfusion and transit time obtained with DASL were independent of the period of the LF and in agreement with previous measurements. In that earlier work, it was suggested that the temporal response of a pixel (i.e., its dynamic characteristics) would depend on the arterial, tissue, and venous contents. For example, the response of arterial pixels to the LF would be expected to be characterized by a short delay (i.e., transit time) and a short time constant (i.e., apparent longitudinal relaxation time), while the response of tissue pixels would be characterized by a larger delay (i.e., transit time) and a time constant comparable to the tissue T_1. Finally, the response of venous pixels to the LF would have the longest transit times, and both the time constant of the response and the amplitude of the response would depend on the water extraction fraction (12). In other words, the time constant of the dynamic response of a voxel should only match the tissue T_1 in the absence of any major vessel in that same voxel.

In this study, an echo planar imaging (EPI) sequence (13) is used in conjunction with the DASL scheme to demonstrate the feasibility of producing simultaneously transit time, longitudinal tissue relaxation time, and perfusion maps. Experiments are performed at 4.7 T on the rat brain during graded hypercapnia. The responses to the LF of voxels containing predominantly arteries or veins are analyzed and discriminated based on differences in responses to the periodic LF. Finally, using the perfusion data obtained during graded hypercapnia, CO_2 reactivity maps are computed for all the parameters measured with DASL.

Theoretical Background

The basic theoretical developments of DASL have been previously described (1). The main equation and the parameter definitions are briefly described here. Water is assumed to be a freely diffusable tracer, and plug flow is assumed between the labeling plane and the exchange site. Given a square LF, of period 2Δ, the response of the tissue magnetization to the LF is given for the case of saturation of macromolecular spins by:

$$\frac{dM_t(t)}{dt} = \frac{M_t^0 - M_t(t)}{T_{1t}} - k_{for}M_b(t) + (1 - 2\alpha_0 e^{-\tau/T_{1a}})\frac{f}{\lambda}M_t^0 - \frac{f}{\lambda}M_t(t) \quad [1]$$

where:

f = tissue perfusion rate.

τ = transit time of the arterial water protons from the labeling plane to the exchange site in the brain.

[1]Laboratory of Functional and Molecular Imaging and NIH MRI Research Facility, National Institute for Neurological Disorders and Stroke, National Institutes of Health, Bethesda, Maryland.

[2]Center for Magnetic Resonance Research, Department of Radiology, University of Minnesota Medical School, Minneapolis, Minnesota.

Grant sponsor: NINDS research program; Grant sponsor: NIH; Grant numbers: RR08079; NS38295; RR03631.

*Correspondence to: Alan P. Koretsky, NIH/NINDS/LFMI, Room 10/B1D118–MSC 1065, Bethesda, MD 20892-1065. E-mail: koretskya@ninds.nih.gov

Received 20 June 2000; revised 15 December 2000; accepted 18 December 2000.

k_{for} = magnetization transfer rate constant between free and bounded tissue protons.

T_{1t} = spin-lattice relaxation time of tissue water protons in the absence of cross relaxation with tissue macromolecular protons (magnetization transfer effects (14)).

T_{1sat} = spin-lattice relaxation time of tissue water protons in the presence of cross relaxation with tissue macromolecular protons (magnetization transfer effects). $T_{1sat} = 1/T_{1t} + k_{for} + f/\lambda$ (1).

T_{1a} = spin-lattice relaxation time of arterial water protons in the absence of cross relaxation with macromolecular arterial protons. $T_{1a} = 1.6$ sec was used (data not shown). Based on the work of Dousset et al. (15), the magnetization transfer effects in the flowing blood were neglected.

M_t = longitudinal magnetization of tissue water protons per gram of brain tissue.

M_t^0 = equilibrium value of M_t.

λ = brain:blood partition coefficient for water. λ = 0.9 ml/g was used (16).

$\alpha(t)$ = labeling function (LF). α_0 is the degree of labeling in the carotid when labeling has been continuously applied. Previously measured values of $\alpha_0 = 0.8$ were used (1,17).

The solution of Eq. [1] in the time domain and for one period of the LF is given by:

for $0 < t \leq \Delta$, $\alpha(t) = \alpha_0$, and for $\tau < t \leq \Delta + \tau$,

$$M_t(t) = M_t^0 T_{1sat}\left[\left(\frac{1}{T_{1t}} + \frac{f}{\lambda}\right) - 2e^{-\tau/T_{1a}}\alpha_0 \frac{f}{\lambda}\left(\frac{(1 - e^{-\Delta/T_{1sat}})e^{-(t-\tau)/T_{1sat}}}{e^{\Delta/T_{1sat}} - e^{-\Delta/T_{1sat}}} + (1 - e^{-(t-\tau)/T_{1sat}})\right)\right] \quad [2a]$$

and for $\Delta < t \leq 2\Delta$, $\alpha(t) = 0$, and for $\Delta + \tau < t \leq 2\Delta + \tau$,

$$M_t(t) = M_t^0 T_{1sat}\left[\left(\frac{1}{T_{1t}} + \frac{f}{\lambda}\right) - 2e^{-\tau/T_{1a}}\alpha_0 \frac{f}{\lambda}\left(\left(\frac{(1 - e^{-\Delta/T_{1sat}})e^{-\Delta/T_{1sat}}}{e^{\Delta/T_{1sat}} - e^{-\Delta/T_{1sat}}} + (1 - e^{-\Delta/T_{1sat}})\right)e^{-(t-\Delta-\tau)/T_{1sat}}\right)\right]. \quad [2b]$$

Numerical simulations of the response of the tissue magnetization to the labeling function, as described by Eq. [2], can be found in Ref. 1. The shape of the tissue response to the LF can be compared to the response of a capacitor to a square current function. The charging (or "filling") time constant of the capacitor can be compared to the tissue longitudinal relaxation time. The main differences between the behavior of a capacitor and that of the brain tissue are: 1) that the tissue response is delayed with respect to the LF (τ being the delay), and 2) that the value of the tissue magnetization at equilibrium is $M_t^0 \neq 0$.

MATERIALS AND METHODS

Rat Preparation

Eight male Sprague-Dawley rats (181 ± 7 g) were initially anesthetized with 5% isoflurane, orally intubated, and then maintained on 2% isoflurane in a 0.75:1.25 O_2:N_2 mixture using a rodent ventilator (Harvard Apparatus, South Natick, MA). The ventilator was set between 55 and 65 strokes.min^{-1} with a stroke volume of 2.0–2.5 cm^3. A catheter was inserted in the femoral artery for monitoring the arterial blood pressure and for sampling arterial blood. Rectal temperature was monitored and maintained at 37 ± 1°C by means of a feedback-controlled flow of heated water. Each rat's body was also covered with a gauze blanket to achieve maximum temperature stability. Head movements were minimized by using a bite bar, ear fixations, and tape on the neck and nose.

Blood samples were withdrawn into heparinized capillary tubes (50 μl each) to minimize systemic effects due to blood pressure reduction; pCO_2, pO_2, and pH were measured by a blood gas analyzer (ABL50; Radiometry, Copenhagen, Denmark). Graded hypercapnia was induced by adding CO_2 (0–6%) to the inhaled gas mixture.

NMR Techniques

All experiments were performed on a 4.7 T (40-cm-diameter bore) driven by a Bruker Avance console and equipped with a Bruker gradient set (15-cm inner diameter, 100 μsec rise time, 17 G/cm max) in the Pittsburgh NMR Center for Biomedical Research at Carnegie Mellon University. A large, RF-shielded, Alderman-Grant transmit RF coil (7-cm diameter) was used for excitation, and a single-loop surface coil (32-mm outer diameter, 22-mm inner diameter) positioned on the top of the rat brain was used for reception. The MR signal was acquired from a single 2-mm-thick axial slice with a field of view (FOV) of 2.56 × 2.56 cm^2.

For all subsequent acquisitions, a gradient-echo-based EPI sequence (single-shot, TE = 12.7 msec, matrix = 32 × 32) was used:

1. T_{1t} measurement. A slice-selective inversion recovery sequence (IR-EPI) was performed to measure T_{1t}, and the following inversion times were used: 0.1, 0.214, 0.334, 0.465, 0.607, 0.766, 0.942, 1.142, 1.374, 1.647, 1.982, 2.413, 3.022, 4.061, and 7.500 sec. A recovery time of 8 sec was allowed prior to the application of the next inversion pulse.
2. T_{1sat} and k_{for} measurements. A saturation transfer sequence was performed. 25 different durations were used for the saturation pulse, ranging linearly between 0.2 and 5.2 sec. A recovery time of 10 sec was allowed prior to the application of the next saturation pulse. Saturation pulses were applied −8500 Hz away from the resonance frequency, with a previously determined amplitude that maximized the magnetization transfer effects (18).
3. DASL measurement. The details of the DASL scheme are given in our previous work (1). A square LF with a period of 4 sec was applied. TR was set to 4.1 sec so that using the interleaved scheme, the apparent temporal resolution was P = 0.1 sec. (If a sinusoidal

function, with a period of 4.0 sec, is sampled with a sampling period of 4.1 sec, it yields the same result as if it was sampled with a period of 0.1 sec. The DASL interleaved scheme is based on this principle, i.e., the use of two different periods that are not harmonic of each other—one for labeling, and the other one for acquiring.) Three periods of the LF were acquired. Arterial spin labeling was generated by flow-induced adiabatic inversion, 2 cm below the slice of interest (labeling frequency = −8500 Hz with respect to the resonance frequency). The control frequency was set to +8300 Hz with respect to the resonance frequency. This value is the average of all the optimal control frequency measured in our previous work (1). The asymmetry around the water frequency was used in order to minimize the effect of the asymmetry of the magnetization transfer spectrum (1,19). For all rats, a DASL data acquisition was performed after death. There were no significant variations in intensity with the LF, as expected (data not shown). This demonstrates that the magnetization transfer effects in tissue generated by the labeling pulse were well corrected for by the control pulse. The amplitude of the labeling and control pulses were the same as the amplitude of the saturation pulse described in the previous saturation transfer experiment, and that was also previously described to yield a labeling degree of about 0.8 (18). No extra crusher gradients were applied so as to allow large vessels to contribute to the signal (20).

Experimental Protocol

Data were acquired as follows, for each of the eight rats:

1. A blood sample was collected for blood gas analysis.
2. T_{1t} measurement.
3. T_{1sat} measurement.
4. Dynamic perfusion measurements were obtained using the interleaved dynamic acquisition scheme (1) with an apparent temporal resolution of P = 100 msec; Δ = 4 sec (0.25 Hz); TR = 4.1 sec. Three LF periods were sampled. The duration of the scan was 3 × 4.1 sec × Δ/P = 8 min 12 sec.
5. Another blood sample was collected for blood gas analysis.
6. Inspired CO_2 was increased, leading to a change in arterial pCO_2 level. After a 10-min delay to reach a physiological steady state, steps 4 and 5 were repeated.
7. The animal was killed by an overdose of ketamine (1 cc).
8. A last dynamic perfusion measurement was made, with the same parameters as before, to check for any residual tissue magnetization transfer.

A total of two inspired CO_2 levels were used: no added CO_2, 3% CO_2, and 6% CO_2 in the inspiration gases for each rat. Two rats did not survive the 6% CO_2 level, but the measurements made without CO_2 and with 3% CO_2 were kept for these two rats. For some rats, different DASL measurements were performed with the same inspired CO_2 level, since the measured arterial pCO_2 was different (gradual drift of the physiological conditions of the animal). The total experiment duration was about 3 hr per rat, during which six blood samples (50 μl each) were collected.

Data Processing

All of the data processing was performed automatically using Matlab 5 (The Mathworks, Inc., Natick, MA) on a Sun Workstation (Sun Microsystems, Inc.). All the fits were performed with a Nelder-Mead type simplex search method (function "fmins"):

1. The T_{1t} maps were computed from the IR-EPI data using a three-parameter fit, based on:

$$M_t(t) = |M_t^0(1 - 2C\exp(-t/T_{1t}))|, \quad [3]$$

   where C corrects for nonperfect inversion. Note that Eq. [3] was fitted to the absolute value of the data.

2. The T_{1sat} and k_{for} maps were computed from the magnetization transfer data using a three-parameter fit, based on:

$$M_t(t) = M_t^0(1 - k_{for}T_{1sat}(1 - \exp(-t/T_{1sat}))). \quad [4]$$

3. The DASL data underwent a previously described baseline correction (1), and the three periods of the LF were averaged to obtain a single period of the tissue response to the LF. This was then Fourier transformed, and the real and imaginary parts of the even components were all set to zero but the continuous component before inverse Fourier transformation. This frequency filtering is based on the intrinsic properties of the LF (the even Fourier components of a single period of a square function are null). Data were fitted in the time domain to Eq. [2], on a voxel by voxel basis, where T_{1sat}, τ, f, and M_b^0 were the fitted parameters. A T_{1sat} map, a perfusion map, and a transit time map were obtained. We will subsequently note the T_{1sat} obtained from DASL $T_{1sat,DASL}$, and the T_{1sat} obtained from the saturation recovery $T_{1sat,recov}$ so that they can be distinguished.
4. For each rat, the change in perfusion as a function of arterial pCO_2, was linearly fitted, on a voxel by voxel basis. The CO_2 perfusion reactivity is expressed in ml/g/min/mmHg.

RESULTS

Figure 1 shows typical data obtained during a DASL experiment and prior to any processing. Fig. 1a shows a typical echo-planar image in the coronal orientation. Figure 1b shows the LF applied at the labeling plane. Figure 1c shows the response of a single voxel in the imaging slice (marked with a black square on Fig. 1a) to the LF. The data show an excellent signal-to-noise ratio.

Figure 2 shows data obtained from three different voxels in the cortex of a rat brain, using the DASL technique. A white arrow on the anatomical image on the side shows the corresponding location. These data are representative of the different dynamic behaviors we observed in each rat

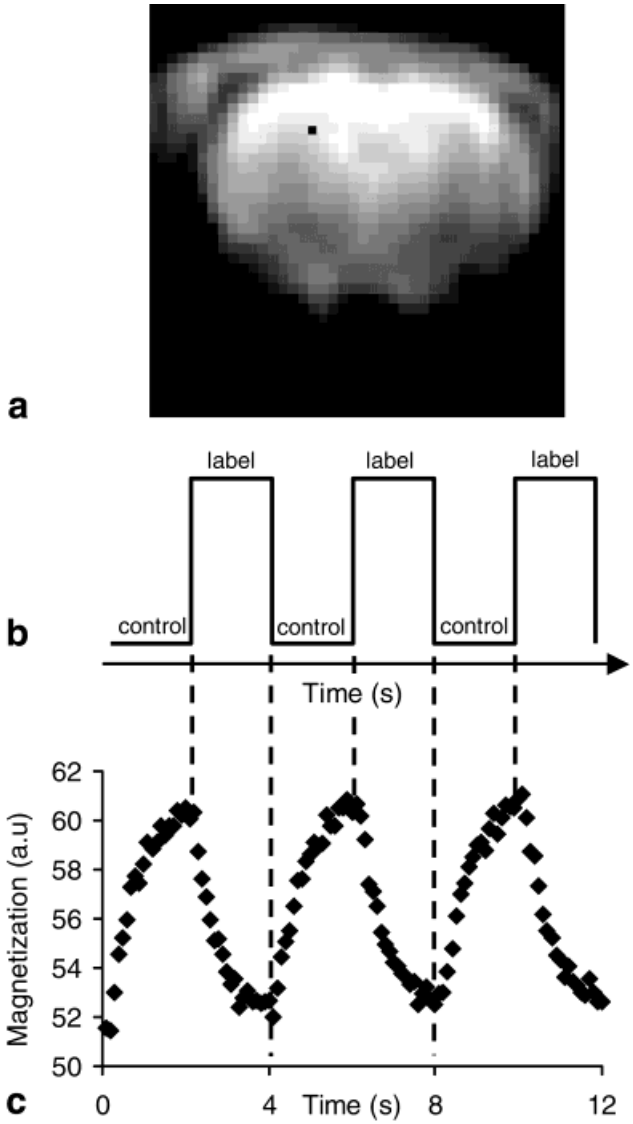

FIG. 1. Raw data from the DASL experiment. **a:** Typical echo-planar image during the DASL acquisition. **b:** Labeling function (LF) applied during the experiment. **c:** Typical response of a single pixel (marked with a black square on image **a**) to the LF, prior to any data processing.

and at multiple locations. The percent change of the signal magnitude (after frequency filtering) and its fit by Eq. [2] are presented for two different arterial pCO_2 values. The corresponding parameter values obtained after fitting the data by Eq. [2] are given in Table 1.

In Fig. 2a, the time constant of the voxel response, $T_{1sat,DASL}$, matches the tissue T_1, $T_{1sat,recov}$. The transit time is between 0.20 and 0.26 sec (Table 1). All three parameters (transit time, time constant of the tissue response, and amplitude of the signal change) vary with the arterial pCO_2. This type of behavior is typical of what is expected for a voxel consisting primarily of normal tissue.

In Fig. 2b, the time constant of the voxel response, $T_{1sat,DASL} = 0.38$ sec, is smaller than $T_{1sat,recov} = 0.62$ sec, and the transit time is small—below the 100 msec temporal resolution used (Table 1). The only parameter that shows a change between the two arterial pCO_2 values is $T_{1sat,DASL}$. This type of voxel behavior can be called "arterial": early blood arrival and fast voxel response (short time constant). If most of the labeled water is located in a large artery, then the value of f does not represent blood flow any more, and the arterial spin-labeling model should not be applied to this particular voxel to quantify blood flow.

In Fig. 2c, the voxel response is slower than the response of the arterial voxel ($T_{1sat,DASL} = 0.55$ sec) but does not

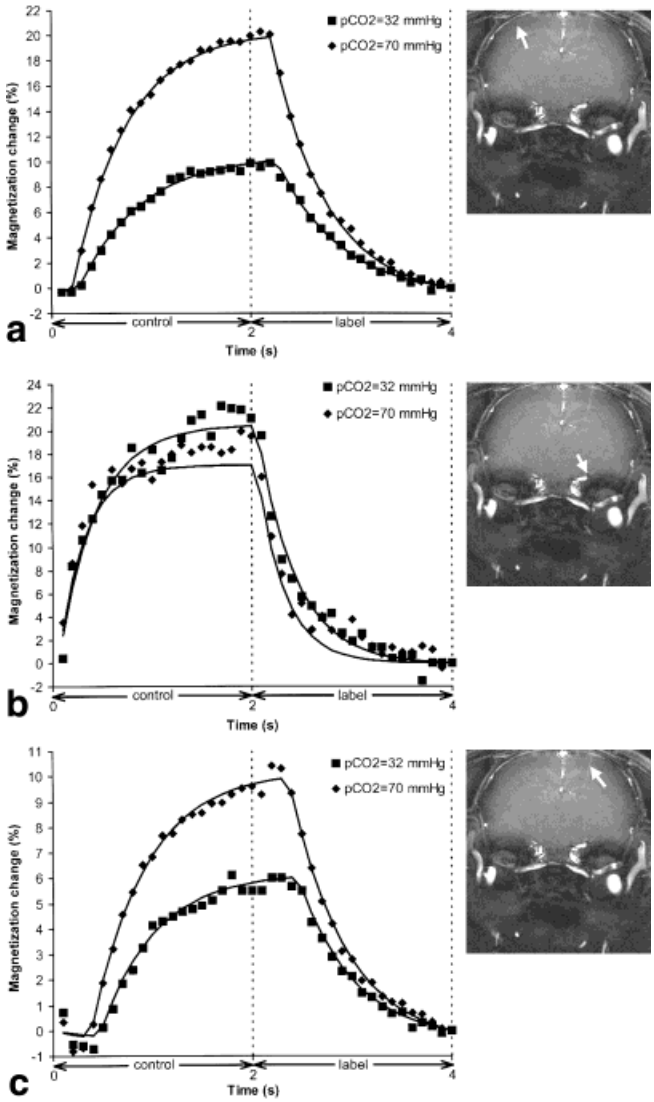

FIG. 2. Time courses of the responses of three different voxels taken in the same rat, at two different arterial pCO_2: (**a**) "tissue" type behavior; (**b**) "arterial" type behavior; and (**c**) "venous" type behavior. On the side of each time course, the corresponding anatomical image, obtained at higher spatial resolution, is presented. A white arrow points to the area in which the time courses were measured. The responses to the three periods of the labeling function (LF) have been averaged to obtain these time courses. Squares and diamonds represent raw data, and continuous lines the best fit of Eq. [2]. The parameter values obtained from the analysis are presented in Table 1. Below the time scale, the arrow indicates the two half-periods of the LF: "control" when the labeling pulse is applied at the control frequency, and "label" when the labeling pulse is applied at the labeling frequency.

Table 1
Analysis of the Dynamic Arterial Spin Labeling Time Courses of Three Different Voxels Taken in the Same Rat, at Two Different Arterial pCO_2*

	pCO_2 (mmHg)	$T_{1sat,recov}$ (sec)	$T_{1sat,DASL}$ (sec)	τ (sec)	f (ml/g/min)
'Tissue' type	32	0.63 s	0.64	0.26	3.87
	70		0.54	0.20	6.57
'Arterial' type	32	0.62 s	0.38	0.04[a]	5.94[b]
	70		0.27	0.04[a]	5.07[b]
'Venous' type	32	0.61 s	0.55	0.46	2.72[b]
	70		0.55	0.37	4.04[b]

*The corresponding time courses are presented in Fig. 3.
[a]Below temporal resolution.
[b]Perfusion values are given for these non tissue-type voxels as an indication of the amplitude of their response to the labeling function.

match the tissue T_1 ($T_{1sat,recov}$ = 0.61 sec). The tissue response is also shifted from the LF by more than 0.37 sec. The time constant of the response does not change with the arterial pCO_2, but both the transit time and the amplitude of the response do: the transit time shortens and the amplitude of the response increases. Note also that the amplitude of the response is small compared to Fig. 2a and b. Because the transit time of this voxel is larger than for voxels taken in the normal brain tissue, and the amplitude of the response is smaller than for other voxels, we assigned this behavior as "venous." Here, again, if most of the labeled water is located in a vein, the value of f does not represent blood flow any more, and thus the arterial spin labeling model cannot be applied to this particular voxel.

Figure 3 shows maps of the different parameters extracted from the DASL measurements. All the images and maps were obtained with an FOV of 2.56 × 2.56 cm^2 on the same rat (slice thickness = 2 mm). Figure 3a shows an angiogram obtained at low arterial pCO_2 with a 256 × 256 matrix. The distribution of large vessels in the slice can be clearly observed. Maps 3b and c were obtained at an arterial pCO_2 of 32 mmHg. Figure 3b shows a perfusion map. Large vessels appear bright in this image. The distribution of flows is in good agreement with the distribution observed by Hansen et al. (21) in the rat brain under isoflurane. Figure 3c shows a transit time map. Some large vessels on the top and at the bottom of the cortex now appear dark, because of the short transit time of blood. These low transit time regions probably appear larger than they actually are, due to our low spatial resolution (partial voluming). However, the transit time map is heterogeneous, underlining the importance of correcting for transit time inhomogeneities when mapping blood flow. It also suggests that a transit time map can contain very useful information.

Figure 3d shows a perfusion CO_2 reactivity map. With a tissue reactivity of about 0.09 ml/g/min/mmHg, and a blood flow at normocapnia of 5.3 ml/g/min, we obtained a reactivity of 0.09/5.3 ~ 1.7%, which is below the measurements reported by Forbes et al. (22). This is most likely due to the high flow observed at normocapnia.

Figure 4 shows the derived values of perfusion, transit time, and $T_{1sat,DASL}$ as a function of arterial pCO_2 level, obtained from all animals. The trends in the parameters are in good agreement with previous measurements (8,20).

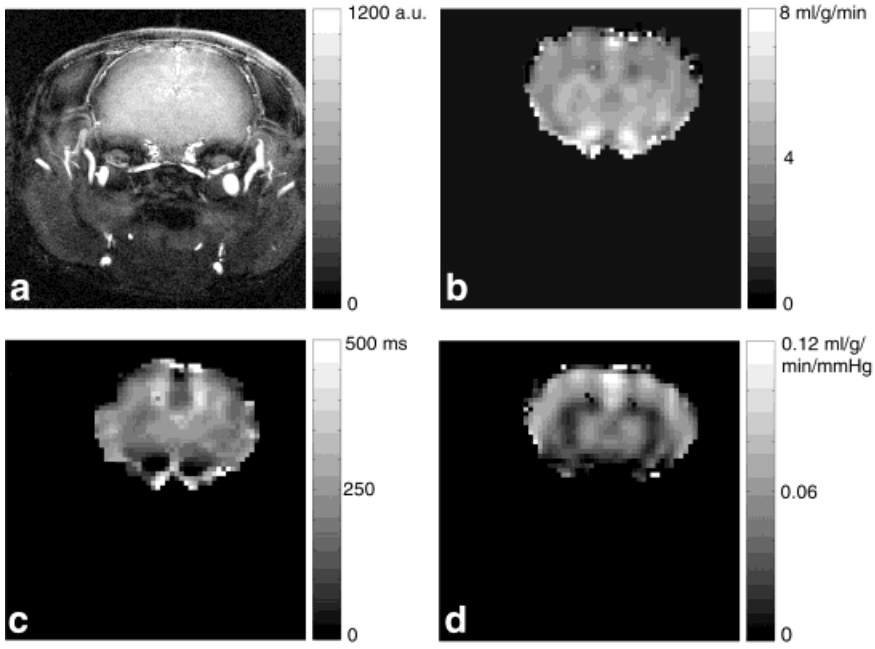

FIG. 3. Images and maps were obtained in an FOV of 2.56 × 2.56 cm^2 on the same rat. **a:** Angiography obtained at pCO_2 = 28 mmHg. Matrix = 256 × 256. All the subsequent maps were obtained with a 32 × 32 matrix and zero-filled to 64 × 64. **b:** Perfusion map. **c:** Transit time map. For **b** and **c**, the arterial pCO_2 was 32 mmHg. **d:** Perfusion reactivity map.

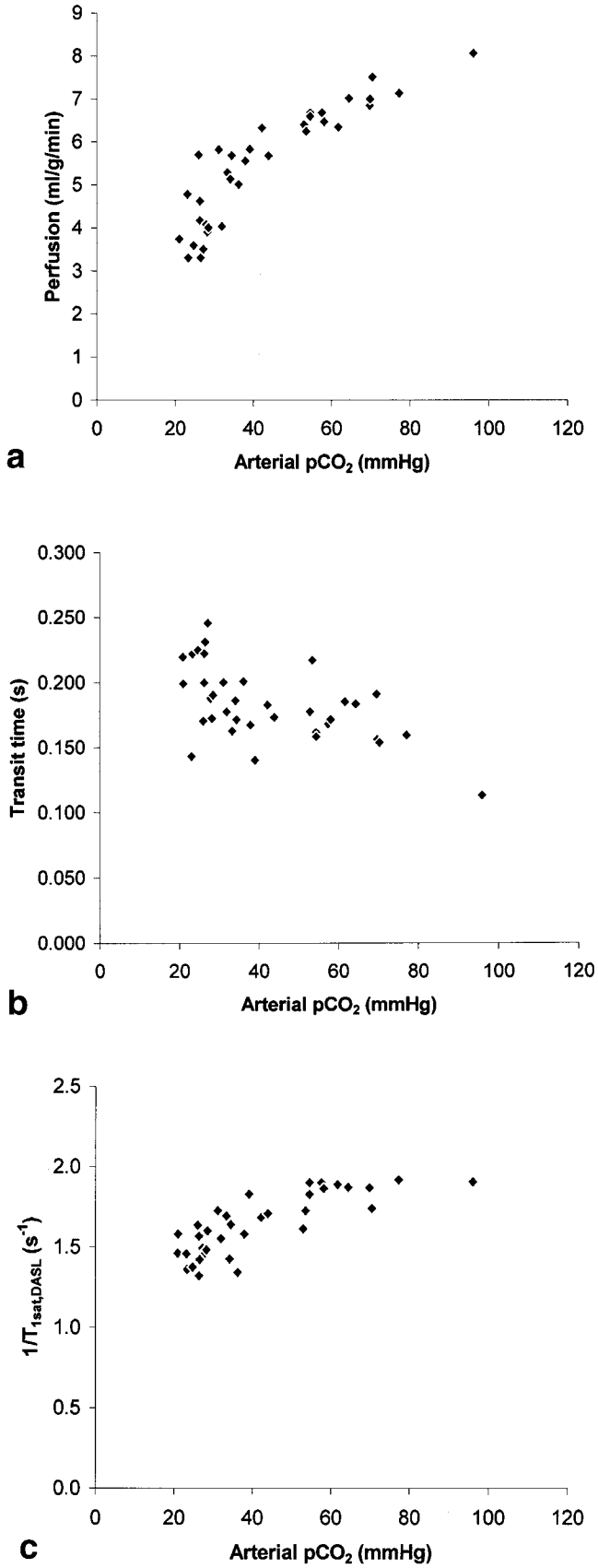

FIG. 4. (**a**) Perfusion, (**b**) transit time, and (**c**) $1/T_{1sat,DASL}$ in the rat brain as a function of arterial pCO_2. Each point represents a single DASL acquisition on a single rat and at a single arterial pCO_2.

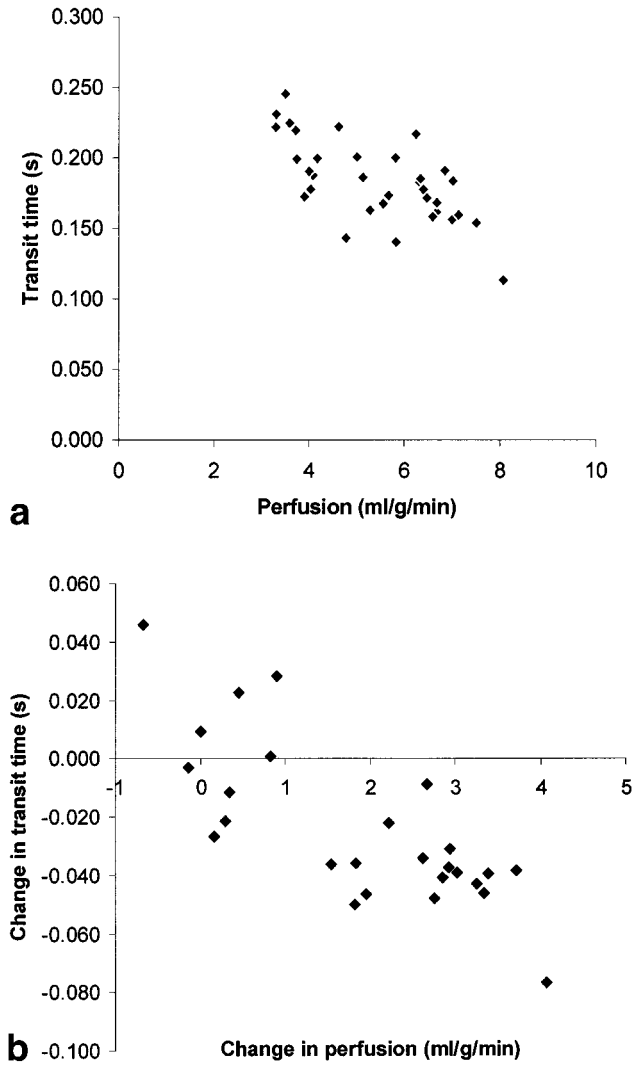

FIG. 5. **a:** Blood transit time as a function of blood perfusion. Each point represents a single DASL acquisition on a single rat. **b:** Change in blood transit time vs. change in blood perfusion for all animals.

The derived values of perfusion (Fig. 4a) show a large increase with arterial pCO_2, as previously reported (1). Since the DASL scheme was used, the quantitative perfusion values obtained have been corrected for the influence of the transit time. The average perfusion value in the cortex at normal pCO_2 (between 30 and 40 mmHg) is 5.3 ± 0.6 ml/g/min. This high value is consistent with the fact that veins respond to the LF (Fig. 2c). This flow value is also in good agreement with other arterial spin labeling measurements under isoflurane (8,23).

Transit time values at normal pCO_2 (Fig. 4b) are in good agreement with those previously measured by Zhang et al. (8) using arterial spin labeling, and with our previous study (1). Transit time decreases as the pCO_2 increases, as expected. Figure 4c shows $1/T_{1sat,DASL}$, and it is clearly visible that $1/T_{1sat,DASL}$ increases with arterial pCO_2. This is predicted by the perfusion model (Eq. [2]) and was originally used to measure flow changes in the human visual cortex (4). This relation was verified in the heart by Williams et al. (24).

Figure 5a shows the transit time as a function of perfusion, and Fig. 5b shows the change in transit time vs. the change in perfusion. For each rat, changes were calculated relative to the initial transit time and perfusion measurements. The change in transit time from the labeling plane to the exchange site appears to decay linearly with the change in perfusion (correlation coefficient = −0.77), and does not seem to reach a plateau at the observed perfusion levels.

DISCUSSION

In this study, we showed that the DASL scheme can be used to produce quantitative maps of the time constant characterizing the inflow of labeled spins in the voxel, the transit time between the labeling plane and the tissue exchange site, and perfusion. It was also observed that voxels in the image exhibit three different types of behavior: a "tissue" type, an "arterial" type, and a "venous" type (Fig. 2). These three types of behavior are defined by a combination of the filling rate and the transit time. Because the spatial resolution at which the data were acquired was low (800 × 800 μm^2 in plane), there was probably significant contamination between the three different voxel types (tissue, arterial, and venous) due to partial voluming effects. If a proper arterial and venous response could be extracted from the image, it should be possible to robustly separate each voxel response into the contributions of arteries, veins, and tissue, allowing angiograms, venograms, and tissue perfusion maps to be derived from the same data set. The fact that different types of response to the labeling function can be seen even at this spatial resolution is extremely promising for future high spatial resolution acquisitions. Using DASL at high spatial resolution should allow for a better separation of arteries, veins, and tissue based on the transit time of labeled blood, and on the time constant characterizing the inflow of labeled water. Moreover, because one should be able to compare amount of labeled spins in veins and in arteries, as well as their respective time constants, it should be possible to derive some information about the extraction fraction of labeled water (12).

Our perfusion measurements agree very well with other groups that have been measuring brain perfusion under isoflurane with arterial spin labeling. Hendrich et al. (8,23) observed a cortical blood flow in the rat cortex at normocapnia of about 4.3 ± 1.0 ml/g/min. However, the values of perfusion measured here are larger than measurements made under other anesthetics, such as halothane (with arterial spin labeling or with other, non-NMR, techniques). For example, measurements in the rat brain under halothane made using ^{14}C-iodoantipyrine by Bereczki et al. (25) yielded an average value of 1.9 ± 0.4 ml/g/min, consistent with arterial spin labeling measurements made under halothane (26).

In the literature, there is no clear consensus about blood flow value in the rat brain measured under isoflurane and under halothane. Using ^{14}C-iodoantipyrine, Young et al. (27) found that the cortical blood flow in the rat was higher under halothane than under isoflurane. Using laser-Doppler, Lee et al. (28) did not observe any differences between anesthetics in the rat cortical blood flow at normal arterial pCO_2. Using arterial spin labeling, Hendrich et al. (23) observed a larger blood flow in the rat cortex at normocapnia under isoflurane than under halothane. Using microscopy, Kusza et al. (29) observed in the cremaster muscle that red blood cells flowed about 30% faster in arterioles of type A1 under isoflurane than under halothane; however, they also reported a larger blood volume under halothane. Although their results cannot be directly applied to the brain, their study suggests that the properties of the microvasculature have to be analyzed in detail to understand the differences observed in blood flow under various anesthetics, using different techniques to measure it. Each technique also has its own sources of errors: ^{14}C-iodoantipyrine-based techniques may suffer from lower extraction fractions at higher flows, or from diffusion of the contrast agent from high concentrated regions (corresponding to high flows) to low concentrated regions (corresponding to low flows) after death and prior to freezing (30). Arterial spin labeling techniques may overestimate the blood flow if the degree of labeling is underestimated, if the tissue T_1 is underestimated (8), if magnetization transfer effects are not properly accounted for (19), if the permeability to water of the blood brain barrier changes with the anesthetic that is being used, or if the signal from large vessels contribute significantly to the signal (20). Arterial spin labeling techniques may underestimate the blood flow if the extraction fraction is not taken into account (12). The fact that venous blood responded so much to the LF indicates that the extraction fraction was less than the 100% expected for the high flow values (5.3 ml/g/min) that we measured. At this flow, Silva et al. (12) measured a water extraction fraction by the tissue of about 45%. However, due to the small contribution of the labeled spins in the vascular pool to the signal, a low water extraction fraction may not affect the quantitative estimation of perfusion (31). For this reason, we did not correct the quantified perfusion values for low extraction fraction. DASL has the potential of separating all these effects, leading to a better estimate of perfusion.

It is interesting to note that our transit time measurements (~ 200 msec at normocapnia (Fig. 4b)) are close to the measurements of Nakagawa et al. (32), made with ^{51}Cr-labeled red cells. However, Nakagawa et al. measured the mean transit time of the tracer through the slice (arterial transit time + capillary transit time + venous transit time) and not the transit time from the labeling plane to the exchange site, as we measured with DASL. The fact that both their measurements and ours yield the same values of transit time suggests that the largest component of transit time is the time spent by labeled spins in the voxel. This is in agreement with physiological data that report a decrease in blood velocity as the vessel diameter decreases, and is also in agreement with our measurements made in arteries. Lowest blood velocities (and therefore higher transit times) are more likely to be found at the capillary level than in the arteries going from the labeling plane to the tissue. If the component of the transit time between the labeling plane and the slice entrance is small compared to the transit time through the arterial vasculature in the slice, then the error made when computing the transit time in the arterial vasculature in the slice is small as well. In addition, if the transit time is dominated by in-slice voxel

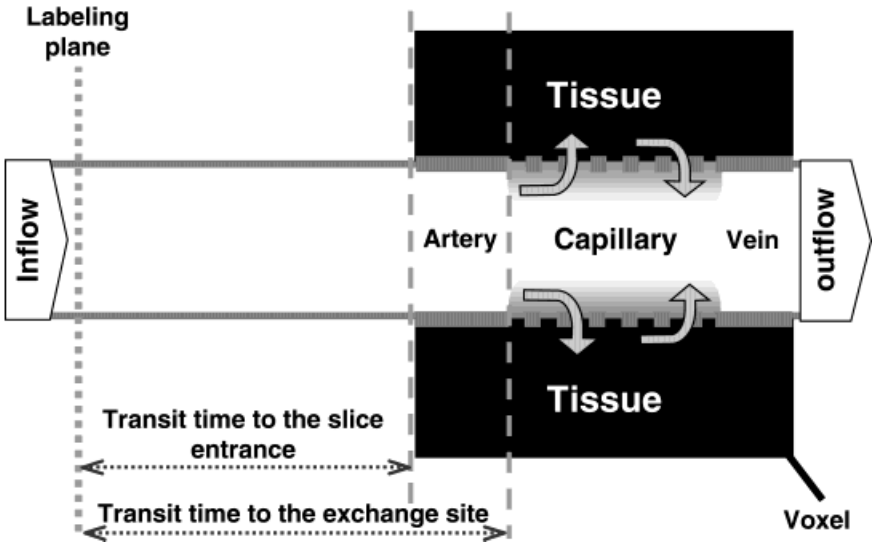

FIG. 6. Pathway of vascular water from the labeling plane to the exchange site. Exchange of water between the vascular compartment and the tissue compartment occurs only at the capillary level. The transit time through the arteries in the voxel, upstream from the exchange site, could be computed by subtracting the transit time to the slice entrance from the transit time to the exchange site. The transit time to the slice entrance could be measured in an artery in the slice of interest, while the transit time to the exchange site could be measured in a voxel that contains primarily tissue.

transit time, then changes in transit time might be a way to characterize changes in regional blood flow due to neuronal activation.

Because DASL allows for a simultaneous determination of blood transit time and blood flow, it should also be possible to use the central volume principle (33), under certain conditions, to compute an estimation of the arterial blood volume. First, between the labeling plane and the exchange site, blood water can be considered as a nondiffusable tracer. There is therefore no loss of tracer of labeled spins between the labeling plane and the exchange site. Second, the blood pathway can be broken in two segments: the first segment goes from the labeling plane to the imaging slice entrance, and the second one from the imaging slice entrance to the exchange site at the tissue. This concept is illustrated in Fig. 6. If one were able to measure the transit time through the second segment (slice entrance to exchange site, MTT), one could derive the arterial blood volume, V, using (33):

$$V = f \times MTT. \quad [5]$$

The ability to measure both the transit time to the slice and the transit "in the slice" is limited by the fact that large vessels either contribute to the signal (absence of crusher gradients) or do not contribute to the signal (use of crusher gradients) (20). Measuring both transit times could be achieved by using DASL with and with crusher gradients. One can also assume that, in the rat brain, the transit time from the labeling plane to the exchange site is dominated by the transit time in the slice, where blood flow is at its lowest velocity. Therefore, measurement made in the absence of crusher gradients should yield an approximate value of the arterial blood volume. Using our transit time and perfusion data, and assuming a transit time to the slice entrance of 40 msec, would yield arterial blood volume fractions between 0.8 and 1.8%, from light hypocapnia to hypercapnia. Assuming a cortical blood volume of 3.4 ± 0.4% (34), the calculated arterial blood fraction at normal arterial pCO_2 would therefore be 24 ± 3%. This value is in good agreement with studies of Neil et al. (35) (29.4 ± 4.3%), van Zijl et al. (36) (21%), and Duong et al. (37) (29 ± 6%).

In summary, we have shown that DASL can be performed using EPI. We have detected different responses to the labeling function used, which we can assign to voxels that are arteries, tissue, or veins. Using DASL at higher spatial resolutions should allow for a better identification of these voxels, and for segmenting the images to generate arteriograms and venograms. It should also enable the quantification of arterial and venous volumes in pixels that are primarily tissue, along with tissue perfusion and transit time measurements.

ACKNOWLEDGMENTS

This was supported by the intramural NINDS research program and by NIH grants RR08079 and NS38295 (S.-G.K.). The authors are indebted to the Pittsburgh NMR Center for Biomedical Research, directed by Prof. Chien Ho, for letting the authors use their 4.7 T system. The Pittsburgh NMR Center for Biomedical Research is supported by NIH grant RR03631.

REFERENCES

1. Barbier EL, Silva AC, Kim HJ, Williams DS, Koretsky AP. Perfusion analysis using dynamic arterial spin labeling (DASL). Magn Reson Med 1999;41:299–308.
2. Detre JA, Leigh JS, Williams DS, Koretsky AP. Perfusion imaging. Magn Reson Med 1992;23:37–45.
3. Edelman RR, Siewert B, Darby DG, Thangaraj V, Nobre AC, Mesulam MM, Warach S. Qualitative mapping of cerebral blood flow and functional localization with echo-planar imaging and signal targeting with alternating radio frequency. Radiology 1994;192:513–520.
4. Kwong KK, Belliveau JW, Chesler DA, Golberg IE, Weisskoff RM, Poncelet BP, Kennedy DN, Hoppel BE, Cohen MS, Turner R, Cheng H-M, Brady TJ, Rosen BR. Dynamic magnetic resonance imaging of human brain activity during primary sensory stimulation. Proc Natl Acad Sci USA 1992;89:5675–5679.
5. Williams DS, Detre JA, Leigh JS, Koretsky AP. Magnetic resonance imaging of perfusion using spin inversion of arterial water. Proc Natl Acad Sci USA 1992;89:212–216.
6. Kim S-G. Quantification of relative cerebral blood flow change by flow-sensitive alternating inversion recovery (FAIR) technique: application to functional mapping. Magn Reson Med 1995;34:293–301.

7. Alsop DC, Detre JA. Reduced transit-time sensitivity in noninvasive magnetic resonance imaging of human cerebral blood flow. J Cereb Blood Flow Metab 1996;16:1236–1249.
8. Hendrich KS, Kochanek PM, Williams DS, Schiding JK, Marion DW, Ho C. Early perfusion after controlled cortical impact in rats: quantification by arterial spin-labeled MRI and the influence of spin-lattice relaxation time heterogeneity. Magn Reson Med 1999;42:673–681.
9. Schlaug G, Benfield A, Baird AE, Siewert B, Lovblad KO, Parker RA, Edelman RR, Warach S. The ischemic penumbra: operationally defined by diffusion and perfusion MRI. Neurology 1999;53:1528–1537.
10. Gonzalez-At JB, Alsop DC, Detre JA. Cerebral perfusion and arterial transit time changes during task activation determined with continuous arterial spin labeling. Magn Reson Med 2000;43:739–746.
11. Frahm J, Merbold K-D, Haenicke W. Localized proton spectroscopy using stimulated echoes. J Magn Reson 1987;72:502–508.
12. Silva AC, Zhang W, Williams DS, Koretsky AP. Estimation of water extraction fractions in rat brain using magnetic resonance measurement of perfusion with arterial spin labeling. Magn Reson Med 1997;38:35–58.
13. Mansfield P. Multi-planar image formation using NMR spin echoes. J Phys C 1977;10:L55–L58.
14. Wolff SD, Balaban RS. Magnetization transfer contrast (MTC) and tissue water proton relaxation in vivo. Magn Reson Med 1989;10:135–144.
15. Dousset V, Degrèze P, Mièze S, Sesay M, Basse-Cathalinat B, Caillé J-M. Magnetization transfer on in vitro circulating blood: implications for time-of-flight MR angiography. J Magn Reson Imaging 1995;5:786–788.
16. Herscovitch P, Raichle ME. What is the correct value for the brain—blood partition coefficient for water? J Cereb Blood Flow Metab 1985; 5:65–69.
17. Zhang W, Williams DS, Koretsky AP. Measurement of rat brain perfusion by NMR using spin labeling of arterial water: in vivo determination of the degree of spin labeling. Magn Reson Med 1993;29:416–421.
18. Zhang W, Williams DS, Detre JA, Koretsky AP. Measurement of brain perfusion by volume-localized NMR spectroscopy using inversion of arterial water spins: accounting for transit time and cross-relaxation. Magn Reson Med 1992;25:362–371.
19. Pekar JJ, Jezzard P, Roberts DA, Leigh JS, Frank JA, McLaughlin AC. Perfusion imaging with compensation for assymetric magnetization transfer effects. Magn Reson Med 1996;35:70–79.
20. Ye FQ, Mattay VS, Jezzard P, Frank JA, Weinberger DR, McLaughlin AC. Correction for vascular artifacts in cerebral blood flow values measured by using arterial spin tagging techniques. Magn Reson Med 1997;37:226–237.
21. Hansen TD, Warner DS, Todd MM, Vust LJ, Trawick DC. Distribution of cerebral blood flow during halothane versus isoflurane anesthesia in rats. Anesthesiology 1988;69:332–337.
22. Forbes ML, Hendrich KS, Kochanek PM, Williams DS, Schiding JK, Wisniewski SR, Kelsey SF, DeKosky ST, Graham SH, Marion DW, Ho C. Assessment of cerebral blood flow and CO2 reactivity after controlled cortical impact by perfusion magnetic resonance imaging using arterial spin-labeling in rats. J Cereb Blood Flow Metab 1997;17:865–874.
23. Hendrich KS, Kochanek PM, Melick JA, Statler KD, Williams DS, Marion DW, Ho C. Characterization of cerebral blood flow during anesthesia with fentanyl, isoflurane, or pentobarbital in normal rats. In: Proceedings of the 8th Annual Meeting of ISMRM, Denver, 2000. p 1277.
24. Williams DS, Grandis DJ, Zhang W, Koretsky AP. Magnetic resonance imaging of perfusion in the isolated rat heart using spin inversion of arterial water. Magn Reson Med 1993;30:361–365.
25. Bereczki D, Wei L, Otsuka T, Hans FJ, Acuff VR, Patlak C, Fenstermacher J. Hypercapnia slightly raises blood volume and sizably elevates flow velocity in brain microvessels. Am J Physiol 1993;264:H1360–H1369.
26. Walsh EG, Minematsu K, Leppo J, Moore SC. Radioactive microsphere validation of a volume localized continuous saturation perfusion measurement. Magn Reson Med 1994;31:147–153.
27. Young WL, Barkai AI, Prohovnik I, Nelson H, Durkin M. Effect of PaCO2 on cerebral blood flow distribution during halothane compared with isoflurane anaesthesia in the rat. Br J Anaesth 1991;67:440–446.
28. Lee JG, Smith JJ, Hudetz AG, Hillard CJ, Bosnjak ZJ, Kampine JP. Laser-Doppler measurement of the effects of halothane and isoflurane on the cerebrovascular CO2 response in the rat. Anesth Analg 1995;80: 696–702.
29. Kusza K, Siemionow M, Nalbantoglu U, Hayes J, Wong KC. Microcirculatory response to halothane and isoflurane anesthesia. Ann Plast Surg 1999;43:57–66.
30. Williams JL, Shea M, Furlan AJ, Little JR, Jones SC. Importance of freezing time when iodoantipyrine is used for measurement of cerebral blood flow. Am J Physiol 1991;261:H252–H256.
31. St. Lawrence KS, Frank JA, McLaughlin AC. Effect of restricted water exchange on cerebral blood flow values calculated with arterial spin tagging: a theoretical investigation. Magn Reson Med 2000;44:440–449.
32. Nakagawa H, Lin S-Z, Bereczki D, Gesztelyi G, Otsuka T, Wei L, Hans F-J, Acuff VR, Chen J-L, Pettigrew KD, Patlak CS, Balsberg RG, Fenstermacher JD. Blood volumes, hematocrits, and transit-times in parenchymal microvascular systems of the rat brain. In: Le Bihan D, editor. Diffusion and perfusion magnetic resonance imaging. New York: Raven Press; 1995. p 193–200.
33. Meier P, Zierler KL. On the theory of the indicator-dilution method for measurement of blood flow and volume. J Appl Physiol 1954;6:731–744.
34. Shockley RP, LaManna JC. Determination of rat cerebral cortical blood volume changes by capillary mean transit time analysis during hypoxia, hypercapnia and hyperventilation. Brain Res 1988;454:170–178.
35. Neil JJ, Ackerman JJ. Detection of pseudodiffusion in the rat brain following blood substitution with perfluorocarbon. J Magn Reson 1992; 97:194–201.
36. Van Zijl PC, Eleff SM, Ulatowski JA, Oja JM, Ulug AM, Traystman RJ, Kauppinen RA. Quantitative assessment of blood flow, blood volume and blood oxygenation effects in functional magnetic resonance imaging. Nat Med 1998;4:159–167.
37. Duong TQ, Kim SG. In vivo MR measurements of regional arterial and venous blood volume fractions in intact rat brain. Magn Reson Med 2000;43:393–402.